Stabilization of tilt order by chain flexibility in Langmuir monolayers

F. Schmid
Institut für Physik, Universität Mainz, D55099 Mainz, Germany
(Received 21 August 1996)

Langmuir monolayers are modeled as systems of short chains, which are confined to a planar surface at one end, but free to move within the plane. The phase behavior is calculated in a mean field approximation, which combines the self consistent field method with elements of classical density functional theory. It is shown that phases with tilt order are unstable in systems of stiff chains, but can be stabilized by chain conformational entropy in systems of sufficiently flexible chains. The chain entropy is also responsible for the appearance of an additional untilted phase, the liquid expanded phase. The region of stability of the different phases is discussed, and their microscopic structure is analyzed in some detail. [S1063-651X(97)11405-2]

PACS number(s): 68.15.+e, 64.75.+g, 68.18.+p, 68.35.Rh

I. INTRODUCTION

Monolayers of amphiphilic molecules have been studied for many years for practical and fundamental reasons. Placed on a solid substrate, they build Langmuir-Blodgett films, which have important technical applications, e.g., in thin film technology [1]. Monolayers of lipids on water are of biological interest, since lipid bilayers—consisting of two weakly coupled monolayers—are essential ingredients of biological membranes [2].

The phase diagram of Langmuir monolayers (monolayers adsorbed at the air water interface) at low surface coverage is qualitatively similar for long chain fatty acids, alcohols, and lipids (Fig. 1) [3,4]. Its most remarkable feature is the presence of two distinct fluid-fluid coexistence regions at intermediate temperatures: the familiar ''gas-liquid'' transition at low surface densities, and an additional transition from a ''liquid expanded'' (LE) phase to a ''liquid condensed'' state at higher densities. The latter is indeed a transition between two fluid states, as shown by the experimental observation that positional correlations in the condensed phase decay exponentially [5]. It is the monolayer equivalent of the ''main'' transition in bilayers, which is interesting from a biological point of view, because it is found at temperatures often close to the body temperature [41.5 °C in L-α-dipalmitoye phosphatidylcholine (DPPC)] [6]. At even higher surface coverage, monolayers can display a rich spectrum of condensed phases, which differ from each other in positional order, tilt order, and orientational order of the backbones of the chains [7,8]. In this work, we shall discuss the condensed phases which can coexist with the expanded phase, i.e. the high temperature untilted phase (LS) and the low temperature tilted phase (L_2, see Fig. 1).

The nature of the transition between liquid expanded and condensed phases has been discussed over many years. In an earlier paper [9], we presented self consistent field calculations of a ''minimal'' model for Langmuir monolayers, where the amphiphilic molecules were modeled as semiflexible chains with one end grafted to a planar surface. We have shown that two ingredients are needed to bring about coexistence between two liquid states: The chain flexibility, which stabilizes the expanded phase, and the chain anisotropy, which dominates the liquid condensed state. The transition is driven by the interplay between the entropy of chain disorder and the energy associated with collective chain alignment. The latter may result from simple packing effects, or from additional (e.g., dipolar) anisotropic interactions between chain segments.

The model hence successfully reproduced the LE and LS phases, yet it seemed to fail to display stable phases with collectively tilted chains. Indications of tilt order were only seen in the unstable regions of two phase coexistence. In that respect, the observed phase behavior was similar to that of grafted rigid rod systems. Grafted rods with fixed grafting points may show tilt order in a region of surface coverage [10,11]. However, the surface energy per chain is higher in the tilted region than in the untilted region. When the rods are given translational degrees of freedom, the tilting transition is therefore replaced by phase separation [12,13].

According to a common picture, tilt order in Langmuir monolayers results from a mismatch between head group and

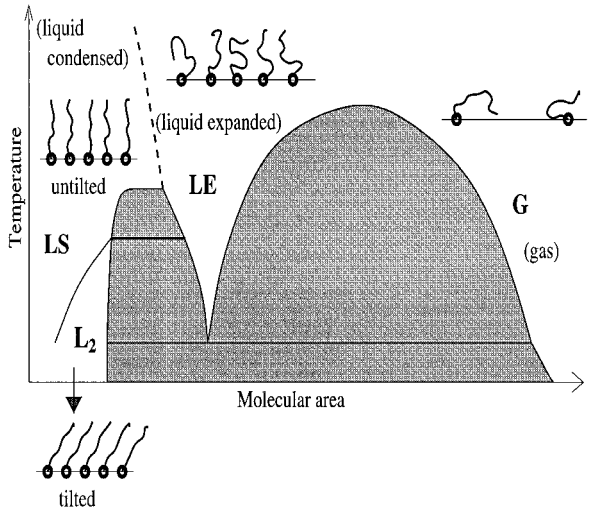

FIG. 1. Phase diagram of Langmuir monolayers at low surface coverage (schematic). The liquid-gas coexistence region is represented in a compressed way relative to the liquid expanded liquid condensed coexistence region. Whether the latter ends in an upper critical, or turns into a second order transition (indicated by the dashed line) in a multicritical point, has yet to be established (after Ref. [3]).

tail segment size. The larger area of the head group constrains the coverage of the condensed phase, and stabilizes surface coverage regions with tilt order. This mechanism is doubtless the driving force for tilt order in many cases, but it is certainly not the only one. For example, it hardly explains the experimental observation of tilt order in monolayers of triple chain phospholipids [14]. Another potential cause for tilt is related to the internal structure of the chains: When the chains are tilted, monomers can ''hook'' into each other, and thus pack more effectively. Presumably, this is responsible for the presence of tilt order in Monte Carlo simulations of endgrafted bead-spring chains [15,16]. Tilt order may also be induced by attractive interactions between the chains and the bare surface [10,17]. However, for hydrophobic $[(CH_2)_n]$ chains on a water surface, that seems less likely.

All these tilting mechanisms do not operate in the minimal model of Ref. [9]. Therefore one would not expect to find tilt order there, unless the model is extended in a suitable way. We shall show that the conformational degrees of freedom of the chains generate another mechanism for the stabilization of tilted states: As we discussed above, giving the chains some flexibility brings a phase into existence, the liquid expanded phase. On making the chains more and more flexible, the condensed phase is also affected: The gain of conformational entropy at lower surface densities compensates in part for the loss of surface energy. As a result, the region of stability of the condensed phase is extended. Provided the chains are sufficiently anisotropic, the coverage at coexistence becomes low enough to support collective tilt.

The influence of conformational chain disorder on tilt in fatty acid monolayers has received some interest recently [18,19]. It has been argued that, in tilted phases, an increase in the number of gauche defects in the chains reduces the tilt angle at the same area coverage. The present work discusses an antipodal, although related effect: Chain disorder stabilizes homogeneous tilted phases at molecular areas, where ordered, straight, chains phase separate into two untilted phases.

The purpose of this work is twofold: to explore the possibilities for tilt order within the minimal model, and to establish a complete phase diagram in terms of the variables stiffness and chain anisotropy. The parameter region in which tilted phases are stable will be determined, as well as the parameter region in which a liquid expanded and a liquid condensed phase can coexist. Where those two regions overlap, one finds a phase diagram which is very similar to the one sketched in Fig. 1. The paper is organized as follows. The model and the self consistent field method are described in Sec. II. A variant of the model [9] is used, which allows, among other things, for a more detailed study of chain defects. Section III presents the predictions of the self consistent field theory first for flexible chains, then for stiff chains. The properties of the different phases are discussed in some detail (density profiles, nematic order, chain defects), and an overview over the phase behavior is given. The results are summarized in Sec. IV.

II. MODEL

A schematic picture of the model is shown in Fig. 2. The amphiphilic molecules are modeled as chains containing n rodlike tail segments of length l_0 and diameter A_0, and one head segment, which is confined to a planar surface at $z=0$. They are subject to three different types of potentials:

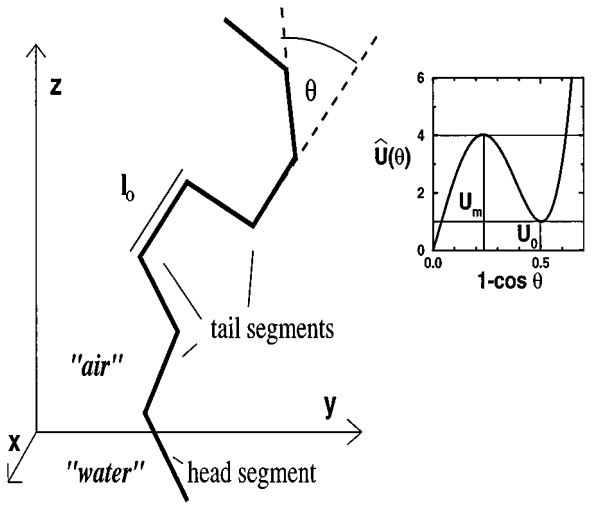

FIG. 2. Schematic picture of the model. The inset shows the functional form of the bending potential.

(i) External potentials, which confine the head segment at $z<0$ and the tail segments at $z>0$.

(ii) A bending potential, which favors parallel alignment of adjacent segments.

(iii) The interactions between segments. Tail segments are anisotropic, have a repulsive hard core, and attract each other at larger distances. Head segment interactions are isotropic and purely repulsive.

The external potentials $h_h^{\rm ext}$ (head segments) and $h_t^{\rm ext}$ (tail segments) are taken to be simply harmonic:

$$\frac{h_h^{\rm ext}(\mathbf{r})}{k_BT}=\begin{cases}0, & z<0\\ k_hz^2, & z>0\end{cases}\quad\text{and}\quad\frac{h_t^{\rm ext}(\mathbf{r})}{k_BT}=\begin{cases}k_tz^2, & z<0\\ 0, & z>0,\end{cases}\tag{1}$$

where k_B is the Boltzmann constant and T the temperature.

The choice of the bending potential is guided by the idea that tail segments in the model chain correspond to two CH_2 groups, each in a hydrocarbon chain. A molecule in an *all trans* conformation is then represented by a completely stretched model chain with bending angles $\theta=0$. A conformation with one *gauche* kink is represented by a model chain, which has one bending angle $\theta=(\pi/3)$ or $\cos\theta=\frac{1}{2}$. In view of these considerations, the bending potential is given the form $U(\theta)/(k_BT)=u\hat{U}(\theta)$, where u is an adjustable stiffness parameter, and

$$\hat{U}(\theta)=25x+34x^2-400x^3+480x^4\quad\text{with}\quad x=1-\cos\theta.\tag{2}$$

The function $\hat{U}(\theta)$ is plotted in Fig. 2. It has a minimum at $\cos(\theta)=\frac{1}{2}$, and takes the value $U_0=1$ there. The relative potential barrier $U_m/U_0\approx4$ has approximately the same height as the energy barrier from *trans* to *gauche* in popular polyethylene models (e.g., by Rigby and Roe [20]). Moreover, the thermal average of $\cos(\theta)$ in a free model chain at $u=1$, $\langle\cos(\theta)\rangle\approx0.7$, is in rough agreement with the value ob-

tained for polyethylene at $k_BT=E_g$, where E_g is the energy of a *gauche* defect [calculated in the rotational isomeric state (RIS) scheme [21]].

The mapping of carbon groups on chain segments should not be taken too literally, since the model is so simple compared to a real hydrocarbon chain. However, the choice of a bending potential with two minima such as Eq. (2) has the advantage that it allows us to define chain defects and to study defect distributions. Note that the energy of *gauche* defects is of order 300 K, i.e., room temperature, in units of the Boltzmann constant k_B. Hence an analysis of their distribution can be instructive, especially in short chains. For most other purposes, a simple harmonic potential such as has been used in Ref. [9] is entirely sufficient, and yields qualitatively the same results.

The interactions between segments are introduced in terms of a functional $\mathcal{F}[\{\hat{\rho}_h(\mathbf{r},\mathbf{w}),\hat{\rho}_t(\mathbf{r},\mathbf{w})\}]$ of the center of mass densities of head ($\hat{\rho}_h$) and tail ($\hat{\rho}_t$) segments with orientation $\mathbf{w}(|\mathbf{w}|=1)$ at position $\mathbf{r}$. The functional includes short range repulsive hard core potentials as well as longer range attractive interaction tails.

In an exact treatment of the above model, one has to perform ensemble averages over all possible configurations of chains, and the corresponding center of mass densities. In this work, we will resort to a local mean field approximation. The densities $\hat{\rho}_{h,t}(\mathbf{r},\mathbf{w})$ are replaced by their ensemble averages, and $\mathcal{F}$ is taken to be a functional of average densities. Single segments interact with others via average fields

$$h^{\mathrm{ind}}_{h,t}(\mathbf{r},\mathbf{w})=\frac{\delta\mathcal{F}}{\delta\hat{\rho}_{h,t}(\mathbf{r},\mathbf{w})}. \tag{3}$$

The effect of local density fluctuations is neglected.

This approximation has a number of important implications. First, correlations between different chains are neglected. The problem therefore reduces to calculating the partition function and the density distribution of a single noninteracting chain (random walk) in the inhomogeneous external fields $h_{h,t}(\mathbf{r},\mathbf{w})=h^{\mathrm{ind}}_{h,t}+h^{\mathrm{ext}}_{h,t}$, which have to be determined self consistently using Eq. (3) (cf. [22,23]). Note that correlations within a chain are still present due to the chain connectivity. Second, the nonintegrable hard core interactions require special treatment. We will choose a common approach in density functional theories [24,25], which is to expand around a reference system of purely repulsive segments. Third, the mean field approximation does not capture the fact that stiff chains are always anisotropic, even if the constituting segments are not. Effective anisotropic interactions result, e.g., from packing effects. Within the mean field approach, they have to be introduced explicitly in terms of an effective segment anisotropy.

Since the segments are extended objects, the center of mass density $\hat{\rho}$ corresponds to a segment mass density

$$\rho_{h,t}(\mathbf{r},\mathbf{w})=\int d\mathbf{r}'K_{h,t}(\mathbf{r}-\mathbf{r}',\mathbf{w})\hat{\rho}_{h,t}(\mathbf{r}',\mathbf{w}). \tag{4}$$

The function $K(\mathbf{r},\mathbf{w})$ reflects the shape of a segment with orientation $\mathbf{w}$. Since the segments are fairly compact, the orientation dependence of the shape function $K(\mathbf{r},\mathbf{w})$ can be neglected, and it is reasonably well approximated by a simple step function.

$$K(\mathbf{r},\mathbf{w})=\begin{cases}1/(l_0A_0), & |z|<l_0/2, \quad (x^2+y^2)<A_0/\pi\\ 0 & \text{otherwise.}\end{cases} \tag{5}$$

We shall also need the total density

$$\rho(\mathbf{r})=\frac{1}{4\pi}\int d\mathbf{w}[\rho_t(\mathbf{r},\mathbf{w})+\rho_h(\mathbf{r},\mathbf{w})], \tag{6}$$

where the integral $\int d\mathbf{w}$ is performed over the full solid angle 4π. With these definitions, we are able to formulate a concrete ansatz for the density functional F. We use a local density approximation, i.e., the functional F is given as the integral over a free energy density function.

$$\frac{1}{k_BT}\mathcal{F}=\int d\mathbf{r}\Bigg\{f_0[\rho(\mathbf{r})]+\frac{1}{32\pi^2}\int\int d\mathbf{w}\,d\mathbf{w}'\times\rho_t(\mathbf{r},\mathbf{w})\rho_t(\mathbf{r},\mathbf{w}')[V(\mathbf{w}\cdot\mathbf{w}')-e]\Bigg\}. \tag{7}$$

The first term describes a reference system of identical segments with isotropic hard core interactions. The free energy density $f_0[\rho]$ is derived from the hypothetical equation of state of a dense melt of such ''ideal'' chain segments: Being part of a chain, the segments have no translational degrees of freedom, and their equation of state has no ideal gas contribution. Furthermore, segments are connected to others at both ends, and therefore they mainly interact within a plane perpendicular to themselves. Hence we assume that their equation of state is reasonably well approximated by the equation of state for hard disks [26], from which the ideal gas term has been subtracted,

$$\Pi(\rho)=\rho\left(\frac{1}{(1-\eta)^2}-1\right), \tag{8}$$

with the reduced pressure $\Pi=p/k_BT$, the density ρ, and the packing fraction $\eta=\rho A_0l_0$. From this one can derive the free energy density using $d(f_0/\rho)/d\rho=\Pi/\rho^2$:

$$f_0[\rho]=\rho\left\{\frac{\eta}{1-\eta}-\ln(1-\eta)\right\}. \tag{9}$$

The second term in Eq. (7) accounts perturbatively for the anisotropic and attractive interactions between tail segments, up to the leading order in the densities. The attractive part of the interaction is absorbed in a single parameter e. The anisotropic part of the interaction is described by an even function $V(x)=V(-x)$, and can be expanded in Legendre polynomials,

$$V(x)=V(-x)=\sum_{l=2,4,\ldots}^{\infty}\frac{2l+1}{4\pi}P_l(x)v_l. \tag{10}$$

We shall neglect all contributions except for the lowest, $v\equiv-v_2$. It should be emphasized again that the anisotropy parameter v cannot necessarily be traced back to an actual anisotropy of single free segments. It is an effective parameter, which has to be introduced in a mean field theory in order to include effects of the chain anisotropy. Thus it has to be identified with an effective anisotropy *per* segment, rather than with the anisotropy *of* a segment.

We complete the definition of the model by specifying the parameters $k_h = k_t = 20/3\, l_0^{-2}$, $e = 40\, l_0^3$, and $A_0 = 2.01\, l_0^2$ (see [9]). This choice is motivated as follows: The parameters k_h and k_t can be chosen arbitrarily, provided they are large enough to ensure the confinement of the heads at the surface, and of the chains above the surface. The strength of the attractive interaction e determines the density within a hydrophobic layer, and affects the jump in the surface coverage at first order transitions. As shown in Ref. [9], e does not have much qualitative influence on the phase behavior; therefore it is not varied systematically here. In a virial expansion, e is given by the integral over the Mayer f function of the attractive interaction, $e = \int (\exp[-v_{\mathrm{attr}}(\mathbf{r})/k_B T] - 1) d\mathbf{r}$. The parameters e and the effective chain diameter A_0 were chosen such that they are compatible with the size and potentials of alkane chains, if one maps two $(CH_2)_n$ groups on one model segment, with alkane potentials taken from Ref. [27].

All calculations were done with chains of tail length $n = 7$. Free model parameters, which were systematically varied, are the stiffness parameter u and the anisotropy parameter v, hereafter given in units of l_0^3. We shall comment briefly on their connection with interaction parameters in other systems, e.g., simulation models. In a simulation, the effective stiffness u can be estimated from matching the thermal average $\langle \cos\theta \rangle$ for the angle θ between adjacent bonds, in a dense melt of free chains, with the average obtained for a random walk of rods with the bending potential $u\hat{U}$, Eq. (2). The least accessible parameter is the effective anisotropy parameter v. As noted earlier, its origin is due mostly to packing effects. A lower bound can be calculated from the excluded covolume (the second virial coefficient) of two stretched chains of the persistence length, divided by the number of segments. In the present model, at $u \sim 1-2$, one obtains $v \sim 10 l_0^3$. Such a calculation, however, neglects the anisotropy in the attractive interaction. Moreover, the segment density in the hydrophobic layer is very high (see Fig. 10), such that higher order virial coefficients come heavily into play. Hence the resulting effective anisotropy will be much higher. In a simulation, v can be determined from the analysis of orientation correlations between segments in a melt of free chains.

The procedure used to solve the problem is similar to the Scheutjens-Fleer method for lattice models of polymers at surfaces [22]. One defines recursively the end segment distributions ($i \leqslant n$)

$$W_i(\mathbf{r},\mathbf{w}) = \frac{1}{4\pi} \int d\mathbf{w}'\, W_{i-1}(\mathbf{r}',\mathbf{w}')\, e^{[-h_t(\mathbf{r},\mathbf{w}) - U(\mathbf{w}\cdot\mathbf{w}')]/k_B T},$$

$$\mathbf{r}' = \mathbf{r} - \frac{l_0}{2}[\mathbf{w} + \mathbf{w}'], \tag{11}$$

$$\overline{W}_i(\mathbf{r},\mathbf{w}) = \frac{1}{4\pi} \int d\mathbf{w}'\, W_{i+1}(\mathbf{r}',\mathbf{w}')\, e^{[-h_t(\mathbf{r}',\mathbf{w}) - U(\mathbf{w}\cdot\mathbf{w}')]/k_B T},$$

$$\mathbf{r}' = \mathbf{r} + \frac{l_0}{2}[\mathbf{w} + \mathbf{w}'], \tag{12}$$

with $W_0(\mathbf{r},\mathbf{w}) = \exp(-h_h(\mathbf{r})/k_B T)$ and $\overline{W_n}(\mathbf{r},\mathbf{w}) = 1$. We consider a homogeneous monolayer of N chains, which each occupy an area per molecule A. Hence we have translational invariance on the xy plane, and the single chain partition function is given by

$$\mathcal{Z}_0 = \frac{1}{4\pi l_0} \int dz\; d\mathbf{w} W_i(z,\mathbf{w}) \overline{W}_i(z,\mathbf{w}), \tag{13}$$

which is independent of i. The center of mass density of the ith segment can be calculated via

$$\hat{\rho}_i(z,\mathbf{w}) = \frac{1}{A l_0} \frac{W_i(z,\mathbf{w}) \overline{W}_i(z,\mathbf{w})}{\mathcal{Z}_0}, \tag{14}$$

and the total free energy per chain (with the de Broglie wavelength λ_B)

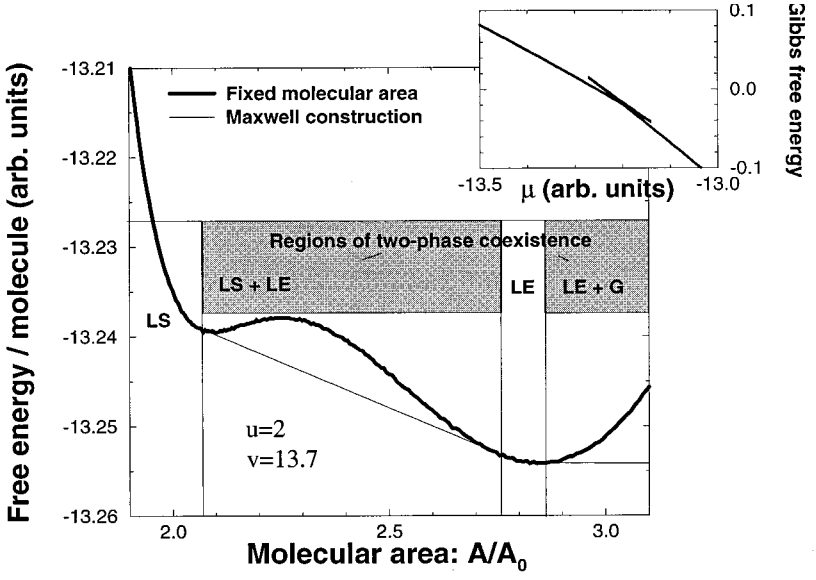

FIG. 3. Free energy per particle vs molecular area at chain stiffness $u = 2$ and anisotropy $v = 13.7$. The thin line indicates the Maxwell construction. The inset shows the Gibbs free energy per area $g/(k_B T)$ vs the chemical potential.

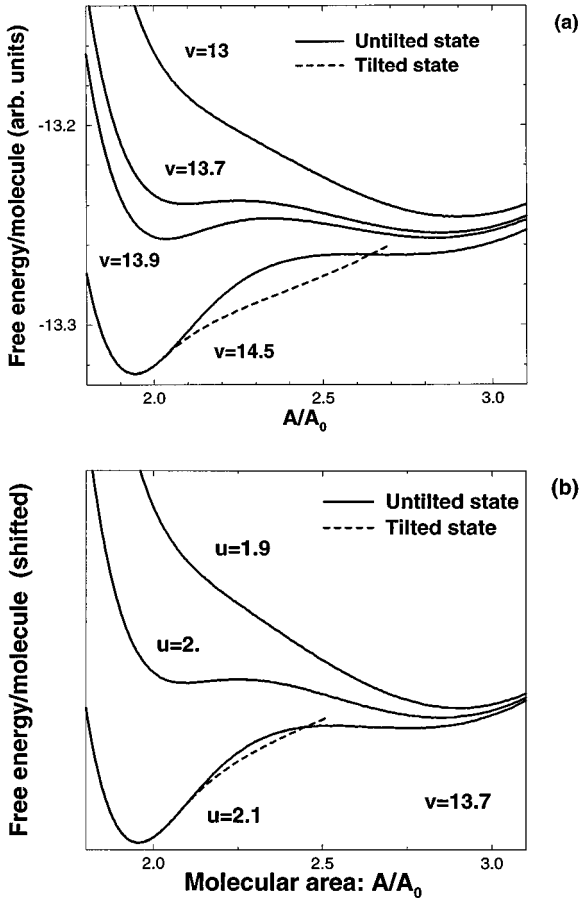

FIG. 4. Free energy per particle vs molecular area (a) for $u=2$ and different values of v; (b) for $v=13.7$ and different values of u. In (a) different offset values have been subtracted from the free energy. A state with tilt order emerges at high chain stiffness or high anisotropy (dashed line).

$$\frac{F}{Nk_BT} = -\ln \mathcal{Z}_0 - \ln(A/\lambda_B^2) - 1 + A\int dz \left\{ \left(f_0[\rho] - \rho \frac{df_0}{d\rho} \right) - \frac{1}{32\pi^2} \int d\mathbf{w}\, d\mathbf{w}' \rho_t(z,\mathbf{w}) \times \rho_t(z,\mathbf{w}')[V(\mathbf{w}\mathbf{w}') - e] \right\}. \quad (15)$$

The chemical potential μ, i.e., the free energy gain on adding one chain, is therefore given by

$$\frac{1}{k_BT}\frac{\partial F}{\partial N} = \frac{\mu}{k_BT} = -\ln \frac{\mathcal{Z}_0 A}{\lambda_B^2}. \quad (16)$$

In the grand canonical ensemble, this leads to the Gibbs free energy per surface area g,

$$\frac{g}{k_bT} = \frac{1}{A}\left(\frac{F}{Nk_BT} - \frac{\mu}{k_BT} \right). \quad (17)$$

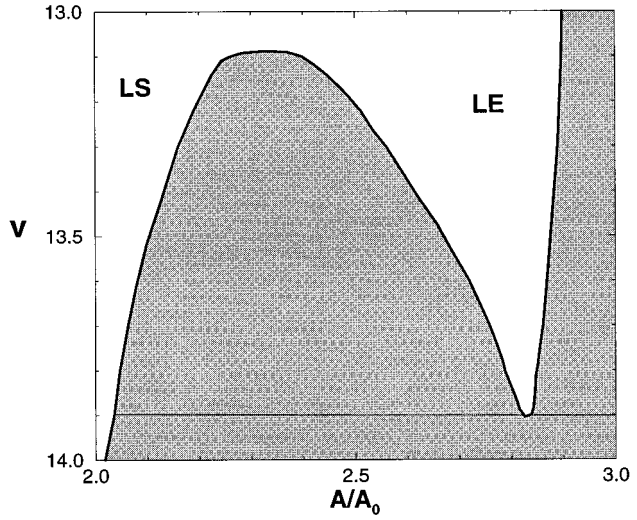

FIG. 5. Phase diagram in the plane of anisotropy v and molecular area A at chain stiffness $u=2$.

Unless stated otherwise, the free energy and the chemical potential will be given in units of k_BT and shifted by $\ln(\lambda_B^2)-1$ in the following.

In practice, it is useful to expand functions of orientation $\mathbf{w}$ in spherical harmonics. Moments up to $l=10$ were taken into account, i.e., 121 functions, a number which proved sufficient. The z direction was discretized in steps of $l_0/5$. The mean field equations were solved iteratively, using the Legendre coefficients of the fields $h_{h,t}^{\mathrm{ind}}(\mathbf{r},\mathbf{w})$ as iteration variables. The iteration procedure combines a method proposed by Ng [28] and simple mixing: Let the vector $\mathbf{x}_n$ be the nth guess of the set of iteration variables, $\mathbf{f}_n$ the fields calculated from there, and $\mathbf{d}_n=\mathbf{f}_n-\mathbf{x}_n$ the remaining deviation. Following Ng, we define the matrix $U_{ij}=(\mathbf{d}_n-\mathbf{d}_{n-i})\cdot(\mathbf{d}_n-\mathbf{d}_{n-j})$ and the vector $V_j=(\mathbf{d}_n-\mathbf{d}_{n-j})\cdot\mathbf{d}_n$, where the dimension of U and V, $i=\max=j_{\max}$, is arbitrary (2–5 in this work). We then invert U, determine the coefficients $A_i=U_{ij}^{-1}V_j$, and calculate $\mathbf{x}_n^A=\mathbf{x}_n+\Sigma_i A_i(\mathbf{x}_{n-i}-\mathbf{x}_n)$ and $\mathbf{f}_n^A=\mathbf{f}_n+\Sigma_i A_i(\mathbf{f}_{n-i}-\mathbf{f}_n)$. In the iteration procedure suggested by Ng, the $(n+1)$th guess of $\mathbf{x}$ is given by $\mathbf{x}_{n+1}=\mathbf{f}_n^A$. Unfortunately, this method does not converge for the present problem. Good results were, however, obtained with the prescription $\mathbf{x}_{n+1}=\mathbf{x}_n^A+\lambda(\mathbf{f}_n^A-\mathbf{x}_n^A)$, with λ ranging between 0.1 and 0.2. A relative accuracy of 10^{-8} was usually reached within less than 100 iteration steps. The iteratively obtained solutions for fixed surface coverage were usually unique, unless metastable states (e.g., tilted states) existed. In that case, the solution with the lowest free energy (15) was selected.

III. RESULTS

A. Stiff chains

Figure 3 shows a free energy curve in a system of relatively stiff chains ($u=2$, $v=13.7$). On increasing the molecular area, the free energy exhibits two minima and then rises. As the area tends to infinity, not shown, it diverges negatively, following the ideal gas term $-\ln(A/\lambda_B^2)$. Hence the Maxwell enveloping function has a negative slope, which guarantees the mechanical stability of the system: The

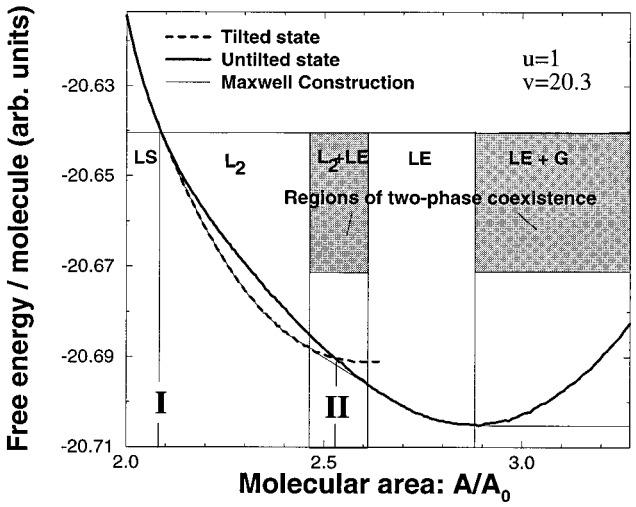

FIG. 6. Free energy per particle vs molecular area at chain stiffness $u=1$ and anisotropy $v=20.3$. Two solutions of the mean field equations are shown, one corresponding to an untilted state (thick solid line), and one describing a tilted state (dashed line). The thin line indicates the Maxwell construction.

spreading pressure $\Pi/k_BT=-\partial F/\partial A\ N^{-1}$ is always positive. The pressure in the gas phase is, however, very low; in the Maxwell construction the common tangent with a coexisting gas phase is practically horizontal. Figure 3 illustrates the situation where one has two distinct regions of phase separation, first between a condensed phase (LS) and an expanded phase (LE), and then between an expanded phase and the gas phase (G). The fact that there is phase separation can be inferred from the Maxwell construction, which does not follow the free energy curve in those two regimes, and from the observation that the Gibbs free energy (17) is not a unique function of the chemical potential (Fig. 3, inset).

If one decreases the chain stiffness u or the chain anisotropy v, the coexisting expanded and condensed phases merge into one at a critical point [Figs. 4(a) and 4(b)]. This point is difficult to locate from just looking at the free energy curves, but can be identified via inspection of the Gibbs free energy as a function of the chemical potential. On increasing u or v, on the other hand, the free energy minimum belonging to the condensed phase decreases relative to the other minimum. A triple point is encountered, beyond which the liquid expanded state is metastable, and the condensed phase coexists with the gas phase. A state with collective tilt emerges in the unstable surface coverage region. Tilt order thus occurs in a system of fixed grafted chains, but is replaced by phase separation when the chains are allowed to move.

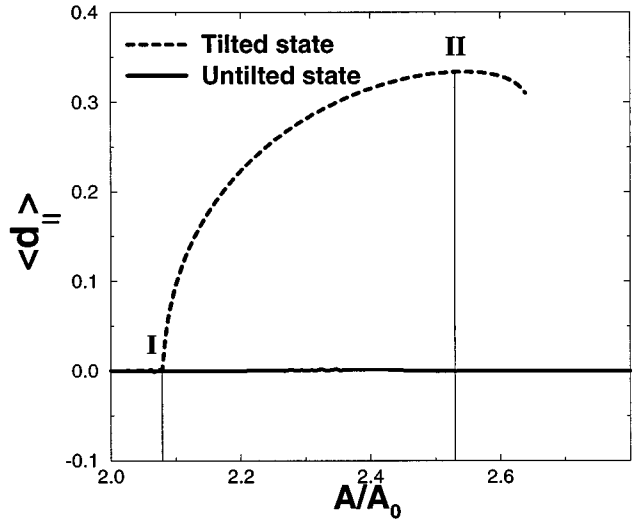

FIG. 7. In-plane alignment of segments $d_\parallel$ vs molecular area at $u=1$ and $v=20.3$. The solid line corresponds to the untilted state, the dashed line to the tilted state. At a fixed grafting density, the tilted state is stable in the coverage region between I and II.

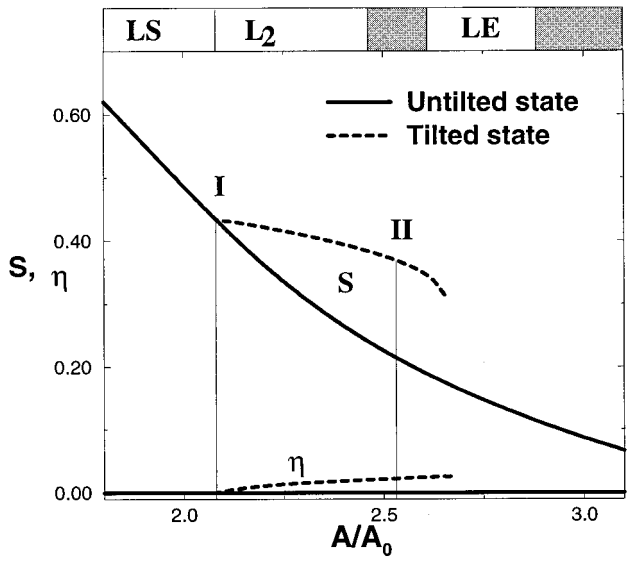

FIG. 8. Nematic order parameter S and biaxiality η vs molecular area at $u=1$ and $v=20.3$. The solid line shows results for the untilted state, the dashed line for the tilted state. Also indicated are the locations of the tilting transitions I and II at a fixed grafting density, and of the coexistence regions between liquid phases in systems of mobile chains.

So far, our results essentially confirm and complete the results reported in Ref. [9]. Systems of relatively stiff chains

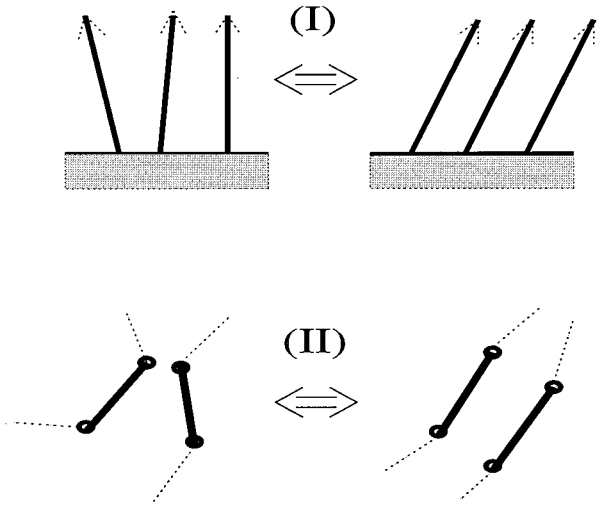

FIG. 9. Types of tilting transitions (see the text for an explanation).

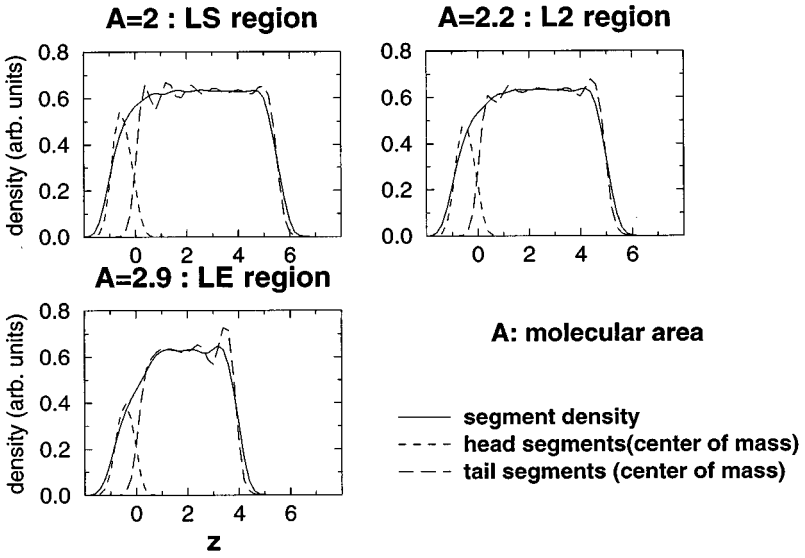

FIG. 10. Density profiles of the monolayer in the direction z perpendicular to the interface, at $u=1$ and $v=20.3$ in different phases (different molecular areas A). Long and short dashed lines show the center-of-mass densities of tail and head segments $\hat{\rho}_{h,t}(z)$, respectively; the solid line shows the total segment density $\rho(z)$.

show qualitatively the same behavior as found earlier in a somewhat different model. Hence we shall not discuss this regime in more detail. The phase diagram in the plane of anisotropy vs molecular area at chain stiffness $u=2$ is shown in Fig. 5.

B. Flexible chains

The transition between the condensed and expanded phases is governed by the interplay of chain flexibility and chain anisotropy. In systems of more flexible chains, one recovers two phase coexistence if the higher conformational entropy is compensated for by higher effective segment anisotropy.

Free energy curves for the set of parameters $u=1$ and $v=20.3$ are shown in Fig. 6. As in Fig. 3, there are two successive first order transitions between fluid phases, passing from the gas phase (G) via a liquid expanded phase (LE) to a liquid condensed phase (L_2). Contrary to the case of stiffer chains, however, the coexisting condensed phase is tilted. Upon further compression of the monolayer, an additional continuous transition to an untilted state (LS) takes place.

The tilt order can be measured in terms of the in-plane alignment of segments, $d_{\parallel}=\sqrt{\langle w_x\rangle^2+\langle w_y\rangle^2}$. The fact that $d_{\parallel}\neq 0$ implies that the symmetry in the xy plane is broken. Figure 7 demonstrates that the ''tilted state'' indeed displays this kind of azimuthal order. In systems of fixed grafted chains, the tilted state is stable in a coverage interval, bounded by a continuous transition at high coverage (marked I in Figs. 6–8) and by a first order transition to the untilted state at low coverage (marked II). When the chains are given lateral mobility, this second transition disappears in the coexistence region of the L_2 and LE phases.

Further insight can be gained from an inspection of the nematic order in the system. The relevant quantity here is the traceless ordering matrix [29] $\mathbf{S}=\langle 3w_iw_j-\delta_{ij}\rangle/2$. It has the eigenvalues $\{S,-(S-\eta)/2,-(S+\eta)/2\}$, with the nematic order parameter S and the biaxiality η. The nematic order S is always nonzero, since the chains are always aligned to some extent in the direction perpendicular to the surface. As the molecular area increases, it decreases monotonically in both the tilted and untilted phases, yet it stays higher in the tilted phase. At the first order transition (II), S jumps from 0.37 in the tilted phase to 0.21 in the untilted phase. The value of S in the tilted state is thus comparable to its value in the nematic phase of liquid crystals, right at the transition to the isotropic phase ($S=0.43$ in the Maier-Saupé model [29]). The in-plane symmetry breaking is reflected by the behavior of the biaxiality, which is nonzero only in the tilted state.

From these results the nature of the tilting transitions in the system can be inferred. The discontinuous low coverage transition (II) is associated with ordering and/or disordering of single segments. It is thus essentially a a nematic-isotropic transition, analogous to those found in liquid crystals. The continuous high coverage transition (I), on the other hand,

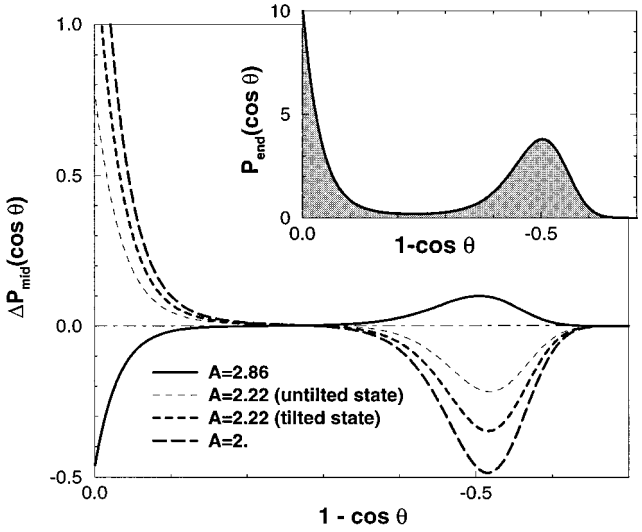

FIG. 11. Difference between the distribution of bending angles $P(\cos\theta)$ in the middle (i.e., between second and third tail segments) and at the end of the chains, $\Delta P_{\mathrm{mid}}(\cos\theta)=P_{\mathrm{mid}}(\cos\theta)-P_{\mathrm{end}}(\cos\theta)$. Results are shown for the parameters $u=1$ and $v=20.3$, and for different states (stable or unstable) at different molecular areas A. The inset shows the distribution P_{end} of the outermost angle, which was identical in all cases.

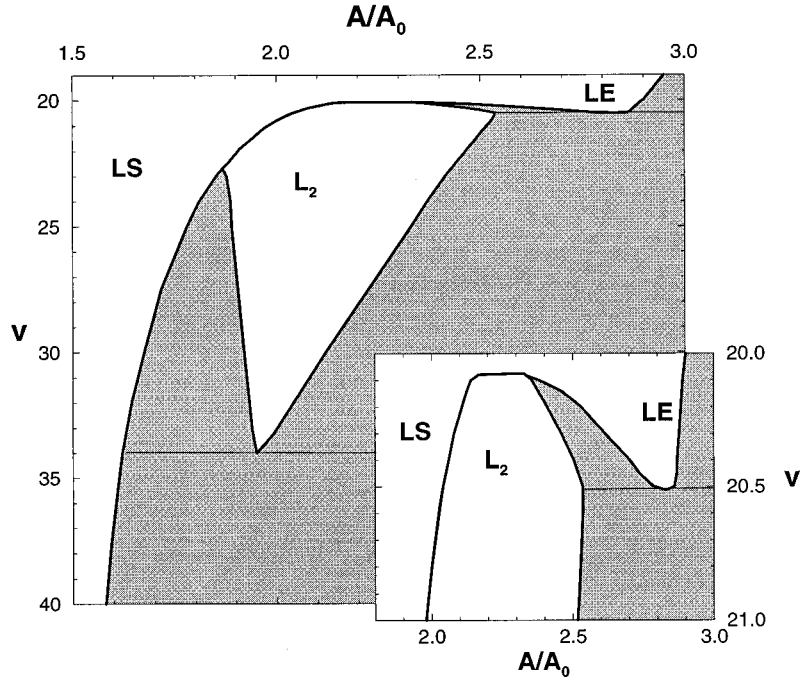

FIG. 12. Phase diagram in the plane of anisotropy v and molecular area A at chain stiffness $u=1$. The inset shows a blowup of the region where the liquid expanded phase is stable.

results from in-plane ordering and/or disordering of whole chains. The surface induces an orientation direction; hence the transition is of XY type [30]. The two types of transitions are illustrated in Fig. 9.

The structure of the monolayer shall be analyzed in some more detail. The density profiles in the three phases do not differ remarkably from each other. Examples are shown in Fig. 10. The total segment density is constant throughout the layer, and independent of the surface area per chain or the tilt order. It is also independent of the chain stiffness and chain anisotropy, and only determined by the interaction parameter e (not shown). Compression results in thickening of the monolayer.

The distribution of bending angles θ, shown in Fig. 11, is more interesting. It has by construction two maxima, one at the bending angle $\theta=0$ and one at $\cos\theta=0.5$. The area under the second maximum gives the concentration of conformational (*gauche*) defects in the chains. As demonstrated in the inset, the distribution for the outermost angle, the angle between the last two segments, is always the same up to the molecular areas which were considered. The main graph shows the deviations from this distribution for the inner angles. In the expanded phase, chains have more defects in the middle than at the ends, i.e., they are more disordered there. In the condensed phases, in contrast, the conformational order is highest in the middle. This result is in agree-

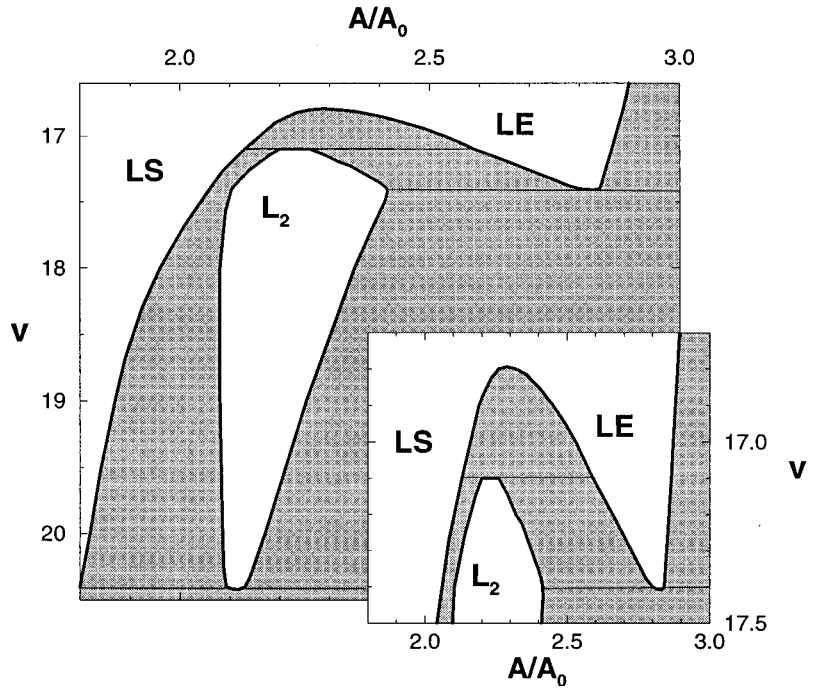

FIG. 13. Phase diagram in the plane of anisotropy v and molecular area A at chain stiffness $u=1.5$.

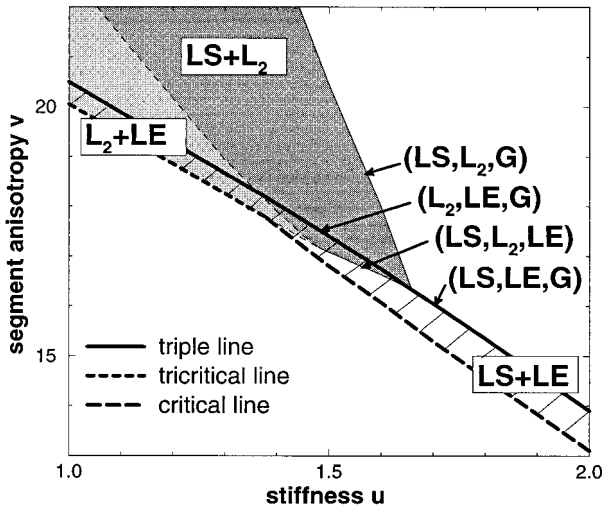

FIG. 14. Projection of the phase diagram in anisotropy v, chain stiffness u, and molecular area A into the (u,v) plane. Short dashed lines indicate multicritical lines, long dashed line critical lines, and the solid lines are triple lines, where three phases can coexist as indicated. Shaded areas are parameter regions where tilted phases can be stable. Coexistence of liquid phases is found in the hatched area (expanded phase and one of the condensed phases) and in the dark shaded area (tilted and untilted condensed phase). See the text for a further explanation.

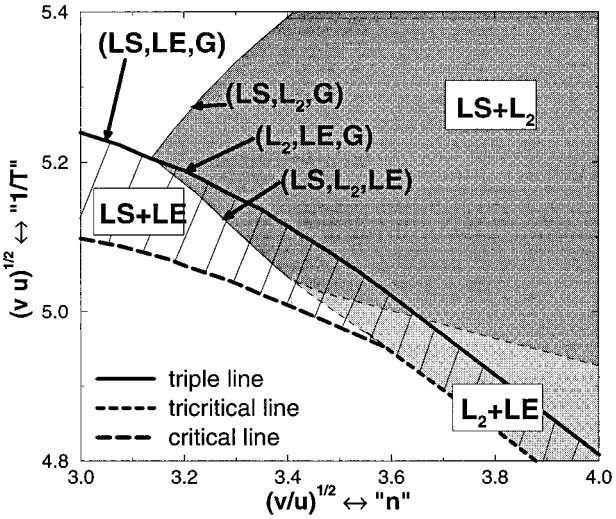

FIG. 15. Same as Fig. 14, with different axis variables. See the text for an explanation.

ment with molecular dynamics simulations [31,32] and other model calculations [33].

We close this section with the discussion of the phase diagram at chain stiffness $u=1$ (Fig. 12). At low chain anisotropy v, there is only one single untilted liquid phase, which coexists with the gas phase. A tilted phase L_2 emerges at a tricritical point, $v=20.1$, and separates two untilted liquid regions, the expanded (LE) and condensed (LS) phases. The transition between the L_2 and LS states is continuous at lower values of the anisotropy v, and replaced by phase separation at the tricritical point $v=22.7$. We note that the tilting transition in monolayers of chains with fixed homogeneous grafting density remains continuous. The tilt order parameter vanishes continuously at a critical line, which is, however, hidden in the coexistence region if the chains are mobile. Beyond the triple point, where the liquid expanded phase becomes metastable ($v=20.5$), the region of stability of the tilted phase narrows down and finally disappears at $v=34$.

C. Phase behavior

We have seen that systems of stiff chains exhibit fluid fluid coexistence of two untilted liquid phases, whereas, in systems of flexible chains, the liquid expanded phase coexists with a tilted condensed phase. In an intermediate range of stiffness, one can find both. An example is the phase diagram for chains of stiffness $u=1.5$, shown in Fig. 13. Phase separation between an expanded phase and an untilted condensed phase sets in at the critical point $v=16.8$. A tilted phase emerges at $v=17.1$ in the coexistence region between the expanded and untilted phases. The liquid expanded phase ceases to be stable at the triple point $v=17.4$. The L_2 and LS phases are separated by a narrow coexistence region; in systems of slightly more flexible chains, $u\leqslant 1.45$, the transition can also be continuous in a window of v (see Fig. 14).

Figure 14 summarizes the phase behavior for chain stiffnesses ranging between between $u=1$ and 2. It shows a projection of the three dimensional phase diagram in the (A,u,v) volume into the (u,v) plane. The shaded area designates the region where a tilted L_2 state is stable. The transition from this phase to the untilted LS phase is continuous in the light shaded area, and first order in the dark shaded region (i.e., the two phases phase separate). The light shaded area is thus bounded by two lines of tricritical points. The liquid expanded (LE) phase is stable in the hatched area, which is bounded by a tricritical or critical line, and a triple line. At very large chain stiffness, $u\sim 3.5$, these two lines merge and disappear (not shown). Hence we recover the rigid rod result reported in the literature. Monolayers of rigid rods display neither stable tilted phases nor a liquid expanded phase.

We shall comment on this diagram with a few points. First, monolayers of chains with fixed anisotropy $v,v>16.4$, display tilted phases only if the chains are sufficiently flexible. This substantiates our claim, that tilt order is stabilized by chain flexibility.

Second, the untilted condensed and expanded phases, both fluid, are not fundamentally different from each other. The possibility of, e.g., hexatic order is ignored within our approximations. Such ordering has, however, been reported in the liquid condensed phase of lipid monolayers [5], and is presumably present in our model too. If this is indeed the case, the coexistence between the LE phase and the LS or L_2 phase is expected to end in a multicritical point, and the transition to turn into a continuous transition at lower values of u or v.

Third, the role of temperature has to be discussed. Assuming that the segment density in the monolayer does not change much in the temperature regime of interest, the temperature enters mainly via the chain stiffness u and the chain anisotropy v. These parameters contain the Boltzmann factor $1/k_BT$, and may have a complicated temperature dependence in addition. Let us neglect the latter and take $u,v\propto 1/T$ for

simplicity. Under this assumption, $(vu)^{-1/2}$ is proportional to the temperature, and $(v/u)^{1/2}$ is temperature independent. The second quantity is interesting in its own right, since it can be related to the chain length n: In a continuum approximation, where chains are treated as space curves of length L, $L \propto n$ and stiffness η, $\eta \propto u$ with orientational dependent interactions V, $V \propto v$, it can be shown that only two of these parameters are independent, e.g., (u/n) and (vn) [34]. Hence varying the chain length n has the same effect as varying $(v/u)^{1/2}$. One can speculate that this remains qualitatively true for discrete chains.

The different possibilities for temperature dependent phase behavior can be read off from Fig. 15, which redraws the diagram of Fig. 14 in the axis variables $(v/u)^{1/2}$ and $(vu)^{1/2}$. For example, the phase diagrams at $(v/u)^{1/2}=3$ and $(v/u)^{1/2}=4$ resemble Figs. 5 and 12, respectively. In the neighborhood of the fluid-fluid coexistence region, increasing the ''chain length'' variable $(v/u)^{1/2}$ produces almost the same effect as decreasing the temperature. This fits to the experimental observation that the addition of two (CH_2) groups to a system has a comparable effect to the reduction of the temperature by 10–20 °C [35,36]. At $(v/u)^{1/2}=3.4$, the phase behavior of Fig. 13 is recovered, which is similar to the experimental phase diagram sketched in Fig. 1.

Note that mean field theories generally overestimate transition temperatures. The effect is particularly strong in two dimensional systems, where the fluctuations even prevent the possibility of true long range tilt order [37], and second order tilting transitions are replaced by Kosterlitz-Thouless-type transitions. Hence the phase diagrams cannot be expected to be quantitatively correct, and Fig. 15 gives just a qualitative picture of the phase behavior. This picture could be tested in simulations, by systematic variations of chain length and chain stiffness.

IV. CONCLUSIONS

We have discussed the interplay of chain anisotropy and conformational entropy in simple model systems for Langmuir monolayers: systems of short chains, which are confined to a planar surface at one end. The phase behavior as a function of chain stiffness and effective anisotropic interaction was calculated in the mean field approximation.

We found that systems of chains with fixed grafting points, i.e., fixed homogeneous grafting density, display tilt order in a density interval. It is bounded by a continuous transition to an untilted phase at high coverage, and by a discontinuous transition at low coverage. The high coverage transition involves ordering of whole chains and is of XY type, and the low coverage transition is caused by ordering of segments and is reminiscent of the nematic-isotropic transition in liquid crystals. Note that, beyond mean field theory, long wavelength fluctuations of the direction of tilt destroy the long range tilt order [37]. However, one can still expect quasi-long-range order, i.e., correlation functions decay algebraically.

If the chains are free to move in the plane, tilt order is replaced by phase separation in systems of stiff chains. In systems of flexible chains, tilted phases remain stable to some extent. The conformational entropy of the chains stabilizes tilt order. In fact, it favors phases at lower surface coverage in general, which engenders both tilted phases and an additional untilted phase, the liquid expanded phase.

As a function of the chain stiffness (or, as we have argued, the chain length), one can distinguish between four different regimes.

(a) Very stiff chains (rigid rod limit): Only one first order order transition is found, from the highly diluted gas phase to the untilted liquid condensed phase.

(b) Stiff chains (or short chains): An additional untilted phase appears in a temperature interval. One finds two successive fluid fluid transitions from the gas phase, passing the liquid expanded phase, to the liquid condensed phase.

(c) Chains of intermediate stiffness: Tilted phases can be stable. Depending on the temperature, the liquid expanded phase coexists with either a tilted or an untilted condensed phase.

(d) Flexible chains (or long chains): The liquid expanded phase coexists with a tilted condensed phase. Upon compression of the monolayer, the tilted phase turns into an untilted phase via a continuous or first order transition.

Hence a complex phenomenology is already found in this simple model, which incorporates only a few aspects of the hydrophobic tails in amphiphilic molecules, and entirely disregards the structure of the head groups. The different phases in Langmuir monolayers at low surface coverage are largely recovered.

We conclude that the essential features of the phase behavior of Langmuir monolayers can already be produced by the alkane tails of the surfactant molecules alone. Nevertheless, the head groups have an important influence on the phase diagram. For example, it has been mentioned that tilted phases can be stabilized by a mismatch between head group and tail segment size. This is most likely the dominant tilting mechanism in monolayers of single chain amphiphiles, e.g., fatty acids. Future investigations will have to explore this factor.

ACKNOWLEDGMENTS

I have greatly benefited from discussions with M. Schick, K. Binder, P. Nielaba, H. Lange, C. Stadler, and A. Halperin. P. Nielaba and K. Binder are gratefully acknowledged for practical advice and a careful reading of the manuscript.

[1] G. G. Roberts, Adv. Phys. **34**, 475 (1985).
[2] R. B. Gennis, *Biomembranes* (Springer-Verlag, Berlin, 1989).
[3] C. M. Knobler, Science **249**, 870 (1990).
[4] H. Möhwald, Ann. Rev. Phys. Chem. **41**, 441 (1990); H. M. McConnell, *ibid*. **42**, 171 (1991).
[5] C. A. Helm, H. Möhwald, K. Kjaer, and J. Als-Nielsen, Biophys. J. **52**, 381 (1987); K. Kjaer, J. Als-Nielsen, C. A. Helm, L. A. Laxhuber, and H. Möhwald, Phys. Rev. Lett. **58**, 2224 (1987).

[6] For a review on bilayers, see, for example, M. Bloom, E. Evans, and O. G. Mouritsen, Quart. Rev. Biophys. **24**, 293 (1991).
[7] C. M. Knobler and R. C. Desai, Ann. Rev. Phys. Chem. **43**, 207 (1992).
[8] V. M. Kaganer, I. R. Peterson, M. C. Shih, M. Durbin, and P. Dutta, J. Chem. Phys. **102**, 9412 (1995).
[9] F. Schmid and M. Schick, J. Chem. Phys. **102**, 2080 (1995).
[10] Z. Wang, J. Phys. (Paris) **51**, 1431 (1990).
[11] M. Scheringer, R. Hilfer, and K. Binder, J. Chem. Phys. **96**, 2269 (1991).
[12] S. Shin, N. Collazo, and S. A. Rice, J. Chem. Phys. **98**, 3469 (1992).
[13] M. Li, A. A. Acero, Z. Huang, and S. A. Rice, Nature **367**, 151 (1994).
[14] A. Dietrich, G. Brezesinski, H. Möhwald, B. Dobner, and P. Nuhn, Nuovo Cimento **16D**, 1537 (1994); G. Brezesinski, C. Böhm, A. Dietrich, and H. Möhwald, Physica B **198**, 146 (1994).
[15] F. M. Haas, R. Hilfer, and K. Binder, J. Phys. Chem. **100**, 15 290 (1996).
[16] H. Lange, diploma thesis.
[17] A. Halperin, S. Alexander, and I. Schechter, J. Chem. Phys. **91**, 1383 (1981).
[18] S. Karaborni and G. Verbist, Europhys. Lett. **27**, 467 (1996).
[19] M. Li and S. A. Rice, J. Chem. Phys. **104**, 6860 (1996).
[20] D. J. Rigby and R. J. Roe, J. Chem. Phys. **87**, 7285 (1987).
[21] D. Y. Yoon and P. J. Flory, J. Chem. Phys. **61**, 5366 (1974).
[22] J. M. H. M. Scheutjens and G. J. Fleer, J. Phys. Chem. **83**, 1619 (1979).
[23] I. Szleifer and M. A. Carignano, in *Advances in Chemical Physics*, edited by I. Prigogine and S. A. Rice (Wiley, New York, 1996), Vol. XCIV, p. 165.
[24] S. K. Nath, J. D. McCoy, J. P. Donley, and J. G. Curro, J. Chem. Phys. **103**, 1635 (1995).
[25] F. Schmid, J. Chem. Phys. **104**, 9191 (1996).
[26] E. Helfand, H. L. Frisch, and J. L. Lebowitz, J. Chem. Phys. **34**, 1037 (1960).
[27] J. D. McCoy, S. Mateas, M. Zorly, and J. G. Curro, J. Chem. Phys. **102**, 8635 (1995).
[28] K.-C. Ng, J. Chem. Phys. **61**, 2680 (1974).
[29] P. G. DeGennes and J. Prost, *The Physics of Liquid Crystals*, 2nd ed. (Clarendon, Oxford, 1993).
[30] M. Plischke and B. Bergersen, *Equilibrium Statistical Physics*, 2nd ed. (World Scientific, Singapore, 1994).
[31] M. A. Moller, D. J. Tildesley, K. S. Kim, and N. Quirke, J. Chem. Phys. **94**, 8390 (1991).
[32] S. Karaborni and S. Toxvaerd, J. Chem. Phys. **96**, 5505 (1992); **97**, 5876 (1992); S. Karaborni, S. Toxvaerd, and O. Olsen, *ibid*. **96**, 4965 (1992); S. Karaborni, Langmuir **1993**, 1334 (1993).
[33] J. P. Rieu and M. Vallade, J. Chem. Phys. **104**, 7729 (1996).
[34] F. Schmid and M. Müller, Macromolecules **28**, 8639 (1995).
[35] S. Ställberg-Stenhagen and E. Stenhagen, Nature **156**, 239 (1945).
[36] A. M. Bibo and I. R. Peterson, Adv. Mater. **2**, 309 (1990).
[37] N. D. Mermin and H. Wagner, Phys. Rev. Lett. **17**, 1133 (1966).